

Article

Graphite Felt Electrode Modified by Quaternary Ammonium for Vanadium Redox Flow Battery with an Ultra-Long Cycle Life

Xuejiao Liu ¹, Junping Hu ^{1,*}, Jun Liu ¹, Hongyi Liu ¹, Sha Fu ¹, Xiongwei Wu ^{1,*} and Yuping Wu ² 

¹ School of Chemistry and Materials Science, College of Resources and Environment, Hunan Agricultural University, Changsha 410128, China

² State Key Laboratory of Materials-Oriented Chemical Engineering, School of Energy Science and Engineering, Nanjing Tech University Nanjing, Nanjing 211816, China

* Correspondence: hjp864569039@163.com (J.H.); wxw@hunau.edu.cn (X.W.)

Abstract: Vanadium redox flow batteries (VRFBs) are one of the most attractive devices for grid-scale energy storage due to their advantages of high safety, flexible assembly, and electrolyte-class recycling. However, the conventional graphite felt electrodes usually possess inferior electrocatalytic activity for vanadium ion redox reactions, vastly limiting the rate and lifespans of VRFBs. Herein, we demonstrate a high-rate and ultra-stable vanadium redox flow battery based on quaternary ammonium salt-modified graphite felt electrodes. At a high current density of 200 mA cm⁻², the constructed VRFB exhibited a superior cycling life of up to 1000 cycles. This work affords a straightforward approach for developing efficient, environmentally friendly, and low-cost graphite felt electrodes for ultra-stable and high-rate VRFBs.

Keywords: quaternary ammonium salt; graphite felt; vanadium redox flow battery



Citation: Liu, X.; Hu, J.; Liu, J.; Liu, H.; Fu, S.; Wu, X.; Wu, Y. Graphite Felt Electrode Modified by Quaternary Ammonium for Vanadium Redox Flow Battery with an Ultra-Long Cycle Life. *Inorganics* **2022**, *10*, 208. <https://doi.org/10.3390/inorganics10110208>

Academic Editor: Christian Julien

Received: 29 August 2022

Accepted: 31 October 2022

Published: 15 November 2022

Publisher's Note: MDPI stays neutral with regard to jurisdictional claims in published maps and institutional affiliations.



Copyright: © 2022 by the authors. Licensee MDPI, Basel, Switzerland. This article is an open access article distributed under the terms and conditions of the Creative Commons Attribution (CC BY) license (<https://creativecommons.org/licenses/by/4.0/>).

1. Introduction

With the depletion of fossil energy sources, the application of renewable energy sources for power generation is becoming increasingly widespread. However, owing to the influence of time and climate, the issues of unstable and discontinuous power generation require large-scale energy storage equipment for regulation. Redox flow batteries [1,2] possess high superiority in terms of large-scale energy storage. Among them, VRFBs have already been commercially applied because their electrolytes are all composed of vanadium ions, which have the advantage of extremely strong reversibility of redox reactions, high safety, and a flexible design for independent energy and power [3]. Nevertheless, several issues require continued research in order to improve the electrochemical performance of VRFBs.

Porous biochar is typically used alone or in combination with carbon fiber materials, such as electrodes [4–7], because of their low cost and advantages in being ecologically friendly and recyclable. Specifically, the mainstream electrodes for VRFBs are composed of three-dimensional carbon materials, such as carbon felt, graphite felt, and electrostatically spun carbon fiber. However, the low vanadium ion redox electrocatalytic activity limits the VRFBs' ability to operate at high current densities. To solve these problems, optimizing the performance of the electrodes is the key to developing efficient VRFBs. For example, modified carbon fiber electrodes prepared by electrostatic spinning technology enable high-rate VRFBs with current densities of up to or even higher than 500 mA cm⁻² [8–10]. Unfortunately, the electrostatic spinning process is complex and costly and is currently not suitable for large-scale applications. To obtain low-cost electrodes that meet the needs of VRFBs with excellent performance, electrode modifications, such as elemental doping, metal modification, and etched porosity, have been performed on existing materials, such as carbon and graphite felts. Additionally, electrode porosity plays a crucial role in the performance of VRB. The etching effect makes it possible to obtain different sizes of pores on carbon electrode materials, which play an important role in the electrolyte transport

rate and reaction sites [11–15]. Larger pore size and higher porosity can effectively reduce the concentration polarization of VRFBs while increasing the migration rate of vanadium ions, building carbon-based electrodes with a high electrochemical surface area through the anchoring effect of hydrophilic materials and improving the wettability and electrochemical activity of the carbon electrodes. However, pore building also has uncontrollable specifications in terms of their size and number, while metal and oxide carbon-based modified electrodes with better electrochemical performance have disadvantages, such as being more expensive and having a serious hydrogen evolution reaction, while electrodes doped with nitrogen [16–19], oxygen [20,21], phosphorus [22,23], and boron [24] show a superior electrochemical in VRFBs. The electrochemical performance and the stability of all-VRFBs have been substantially improved. For example, He et al. [10] prepared nitrogen-doped carbon groups by means of urea hydrothermal treatment at temperatures below 180 °C. The surface N doping resulted in increased electronic conductivity, more active sites, and increased hydrophilicity of the carbon groups.

The N atom has a strong electronegativity and combines with the carbon atom to produce a nitrogen negative ion that accelerates the adsorption of VO_2^+ and VO_2^+ in the active site of the reaction. In addition, the N atom has a surplus of lone pair electrons that can create a transition state N-V bond with the vanadium positive ion with empty orbitals, which accelerates the transfer of charge between the catalytic active site and the reactant (Figure 1). In addition, high catalytic activity, wettability, and vanadium ion surface diffusion rates are conducive to reducing the ohmic voltage drop and the voltage loss by lowering the electrode polarization in VRFBs and improving the voltage efficiency of VRFBs.

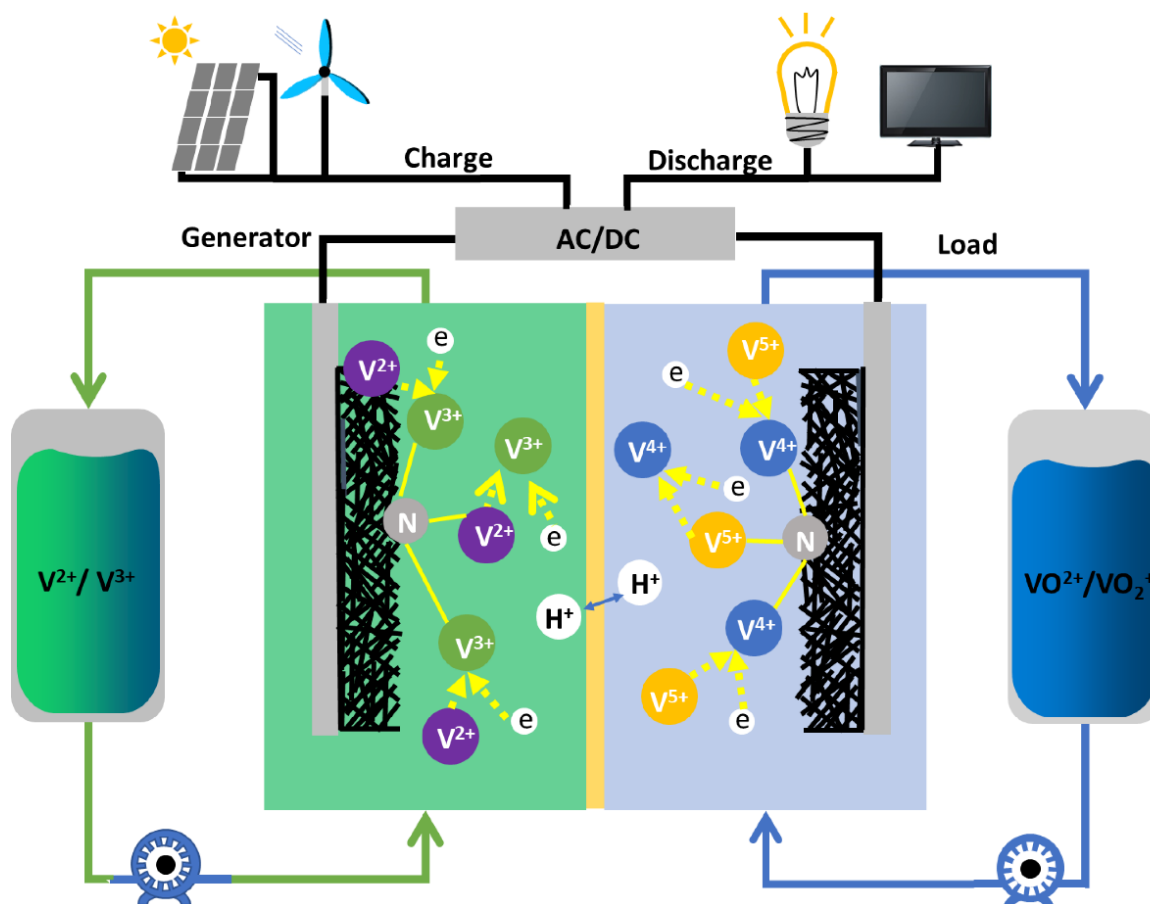


Figure 1. Schematic diagram of the operation of a vanadium redox flow battery with N263-modified graphite felt electrodes.

Herein, we propose quaternary ammonium salts as the nitrogen source to achieve the nitrogen modification of a graphite felt electrode through ultrasonic dispersion and high-temperature heat treatment. The abundant carbon micropores greatly alleviate electrode polarization and charge transfer and reduces the diffusion resistance. The process is simple and inexpensive, reducing the activation energy of the vanadium ion redox reaction and improving the hydrophilic and electrochemical activity of the carbon-based electrode. It is expected that the development of a large-scale electrochemical energy storage technology can be realized for VRFBs.

2. Results

2.1. Morphological Characterization

As shown in Figure 2, the graphite felt treated with methyltrioctylammonium chloride (N263-GF) and the graphite felt electrode without any reagent treatment (GF) both presented defects generated on the surface of the carbon fiber under the same conditions. Interestingly, there were many small particles with a uniform distribution on the surface of the graphite felt treated with N263. These particles were nitrogen-containing carbon nanoparticles fired by N263 under an argon atmosphere at 600 °C during high-temperature heat treatment, which may have increased the specific surface area of the carbon fiber and the active sites of the vanadium ions (see Figure S1).

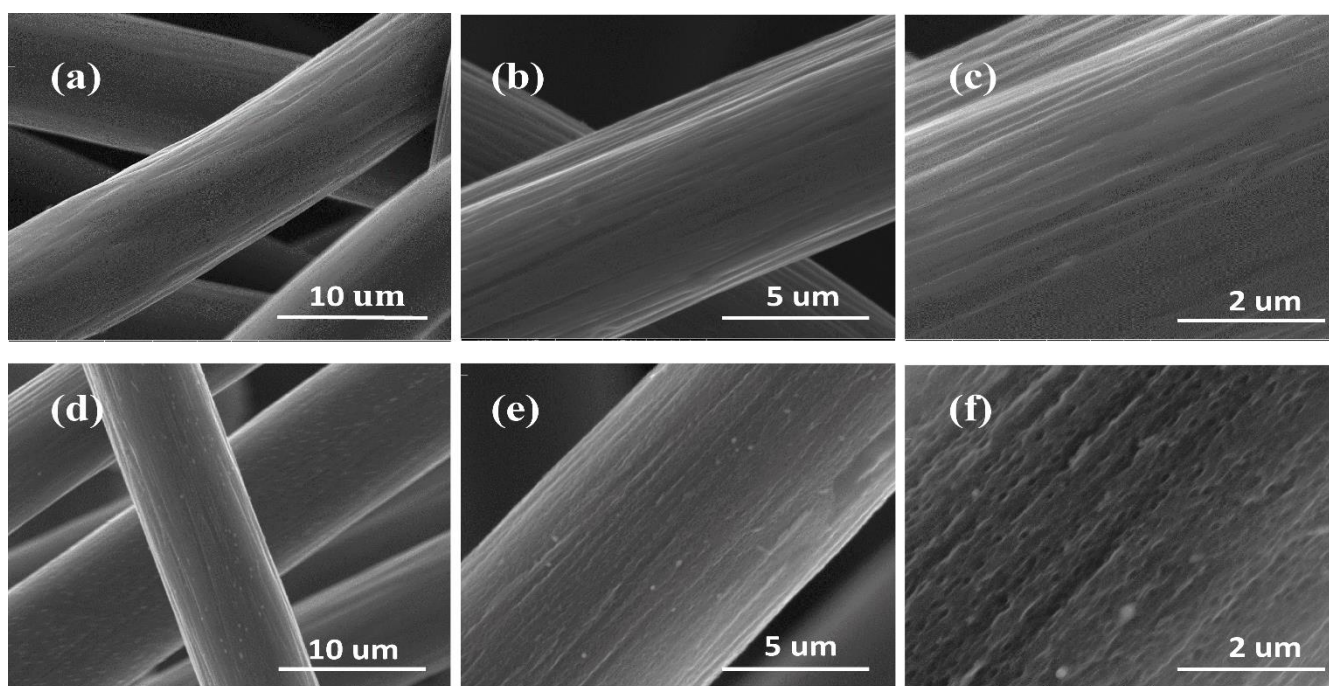


Figure 2. SEM images of the GF (a–c); N263-GF (d–f).

From the elemental distribution diagram in Figure 3a, the N263-GF electrode had a uniform distribution of C, N, and Cl elements on the surface, indicating that N263 was successfully doped on the surface of the graphite felt. We carried out a comparative performance test on N263-GF and GF electrodes wetted with vanadium electrolyte (see Figure 3d–f). On the basis of these results, we found that N263-GF had the best wetting properties, thereby the whole N263-GF sample could be wetted quickly by vanadium electrolyte, while the untreated GF surface showed greater hydrophobicity and floated on the electrolyte surface. In addition, the above results were verified on the basis of the water contact angle test, in which water droplets infiltrated into the interior of the graphite felt after being dropped on the N263-GF surface. Conversely, when the water droplets were dropped onto the GF surface, they were not able to spread on the GF surface and had difficulty

entering the interior. It is illustrated that the presence of a moderate amount of the N element improved the electrode wettability towards the aqueous electrolyte. The high hydrophilicity of N263-GF may reduce the concentration polarization due to the uneven distribution of electrolytes caused by hydrophobicity problems in GF.

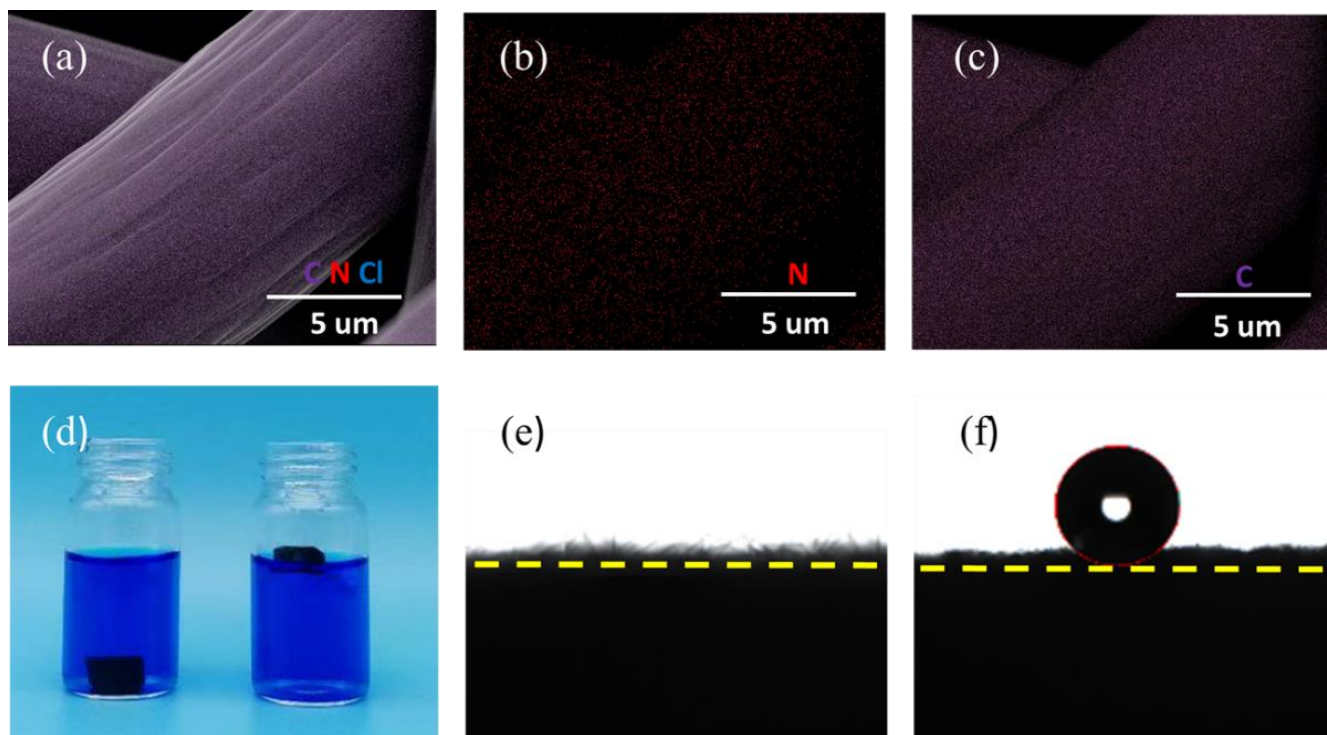


Figure 3. Elemental distribution of N263-GF and electrolyte wettability, water contact angle test (a); C, N, Cl, (b); N, (c); C, (d); N263-GF (left) and GF (right) in the bottle containing electrolyte, and N263-GF (e); and GF (f) water contact angle images.

Figure 4a and Figure S2 show the Raman spectroscopy of the GF and N263-GF samples. Four peaks were found in the 0–4000 cm^{-1} Raman frequency shift interval at a light source wavelength of 532 nm for both GF and N263-GF. One peak at 1350 cm^{-1} was the D band, implying that the carbon material contained sp^2 bonds with hybridization defects. The other peak at 1590 cm^{-1} was the G band, representing the presence of sp^2 bonds in the sample and the presence of graphitized carbon. The ratio I_D/I_G of the D and G band area in the Raman spectrogram represents the degree of defects in the graphene felt, and the defect sites were able to change the electron cloud arrangement outside the carbon atoms and interrupt the Π -bonded conjugation system of graphene. Therefore, the greater the number of defect sites, the more active sites can provide the vanadium ion redox reaction, which is more favorable to the electrochemical performance of VRFBs. In addition, the remaining two peaks at 2690 cm^{-1} and 2930 cm^{-1} were the 2D band and D + D' band of carbon [25–27]. They represent the hierarchical structure of graphite in carbon materials. The fitting analysis of the Raman spectral data using Gaussian distribution shows that the I_D/I_G average values of GF and N263-GF were 1.36 and 1.51, respectively, which indicates that N262-GF had more defects and was able to provide more active sites for the reaction. In addition, when the I_G/I_{2D} values of both samples in Figure 4a were greater than 0.6, it indicated that the samples were composed of multi-layered graphite, which was caused by the graphite felt used for the raw material. In the XRD spectra presented in Figure 4b, two characteristic peaks appear at 10–80°, corresponding to the (002) and (001) planes of graphite [28,29].

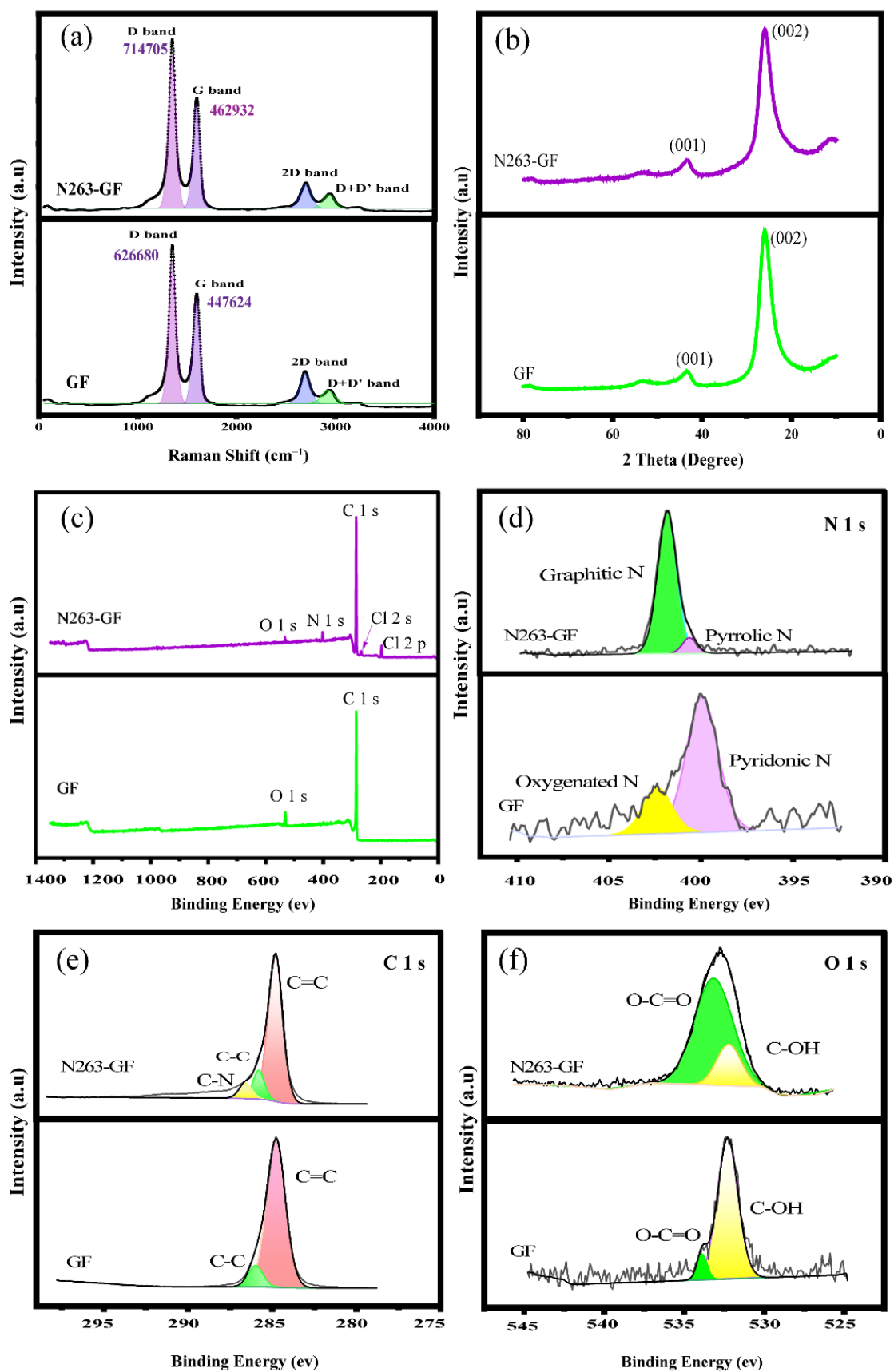


Figure 4. Raman spectra (a), XRD pattern (b), XPS survey scans with various element contents (c), and fitting of the high-resolution N 1s (d), C 1s (e), O 1s (f), of N263-GF and GF electrode materials.

In the XPS full spectrum presented in Figure 4c, it can be clearly seen that N263-GF contains C, N, O, and Cl. The characteristic peaks of C=C (284.4 eV) and C-C (285.9 eV) carbon-containing functional groups appeared in all of the graphite felts, but the C-N (286.2 eV) characteristic peak only appeared in N263-GF, which can be attributed to the presence of nitrogen carbide in the graphite felt (Figure 4d) [30–33]. In addition, the presence of pyrrolic nitrogen (400.3 eV) and graphitic nitrogen (401.8 eV) on the surface of N263-GF can be seen in the N 1 s spectrum of Figure 4e. The higher content of graphitic nitrogen indicates that the successful addition of nitrogen atoms to the surface of the graphite felt fibers increases the defect sites on the surface of the carbon fibers while making the active sites on the surface of N263-GF, which also corresponds to the Raman and XRD results [34–37]. Furthermore, in Figure 4f, the O 1 s orbital information also indicates the presence of C-OH (532.2 eV), O-C=O (533.0 eV–533.9 eV) on the surface of N263-GF and GF electrodes. Among them, the N263-GF electrode material has the majority of O-C=O and high oxygen content, which promotes the activity of the vanadium redox reaction to some extent [29,38,39].

2.2. Electrochemical Test Analysis

GF and N263-GF electrodes were tested by cyclic voltammetry at a scan rate of 10 mV/s and electrochemical impedance spectroscopy through the three-electrode system (Figure 5a,b and Figure S3). The $\text{VO}^{2+}/\text{VO}_2^+$ redox peak current ratio of N263-GF is 0.97, which is closer to 1 than the redox peak current ratio of 0.93 for GF, thus showing an improved reversibility of the positive electrode redox reaction. It is worth mentioning that the difference in the positive electrode peak voltage of N263-GF is 187 mV, which is significantly smaller than GF with a peak potential difference of 264 mV, indicating that an appropriate amount of nitrogen doping can improve the reaction dynamics of the $\text{VO}^{2+}/\text{VO}_2^+$ electric pair and reduce the electrochemical polarization of the electrode.

In the electrode reaction kinetics, the reaction rate of the VRFBs is controlled by the redox reaction of the vanadium ions ($\text{V}^{2+}/\text{V}^{3+}$) at the negative electrode. According to the CV curve of the negative electrode in Figure 5a, the peak current ratio of N263-GF is 0.86, while the redox peak current ratio of GF is 0.34, clearly showing that the electrochemical performance of N263-GF is better than GF. The N element on the surface of N263-GF effectively increases the electrochemical activity of the electrode and improves the surface transport ions and the ability of the electrode. Therefore, we can well conclude that the addition of N263 to the electrode significantly improves the electrochemical performance of the VRFBs. The AC impedance spectra can be analyzed for the charge transfer impedance of the electrode material (Figure S4). By building an equivalent circuit model using Z-view software and then fitting the AC impedance, it can be seen that L is the -90° part of the phase angle in the high-frequency region of the AC impedance spectrum, the inductive resistance of which is caused by the unshielded wire (Figure 5c and Table S2). In addition, R_1 is the ohmic resistance of the whole VOSO_4 electrolyte and electrode, while the R_2 part is the charge transfer resistance of the electrode interface [40,41]. C_1 is the double-layer capacitance formed by the electrode and electrolyte interface; both R_2 and C_1 occur at the same position of the electrode and electrolyte interface, thereby forming a parallel state. The slopes of the Warburg curves of the GF and N263-GF electrodes are not very different, which means that the diameter of the semicircle in the AC impedance spectrum of N263-GF is smaller under the same test conditions. Compared with the GF electrode, the lower charge transfer impedance of the N263-GF electrode indicates a higher charge transfer efficiency, which greatly reduces the interfacial polarization on the electrode surface and improves the conductivity of the electrode.

In general, the ion diffusion coefficient for the vanadium ion reaction can be determined using the Randles Sevcik equation [42–44]:

$$i_p = 2.69 \times 10^5 \text{ An}^{3/2} D^{1/2} \nu^{1/2} C, \quad (1)$$

where i_p represents the redox peak current, A is the electrode reaction area, n is the number of electrons gained or lost per unit in the electrode reaction, D is the diffusion rate of ions, v is the cyclic voltammetry scan rate, and C is the concentration of vanadium ions.

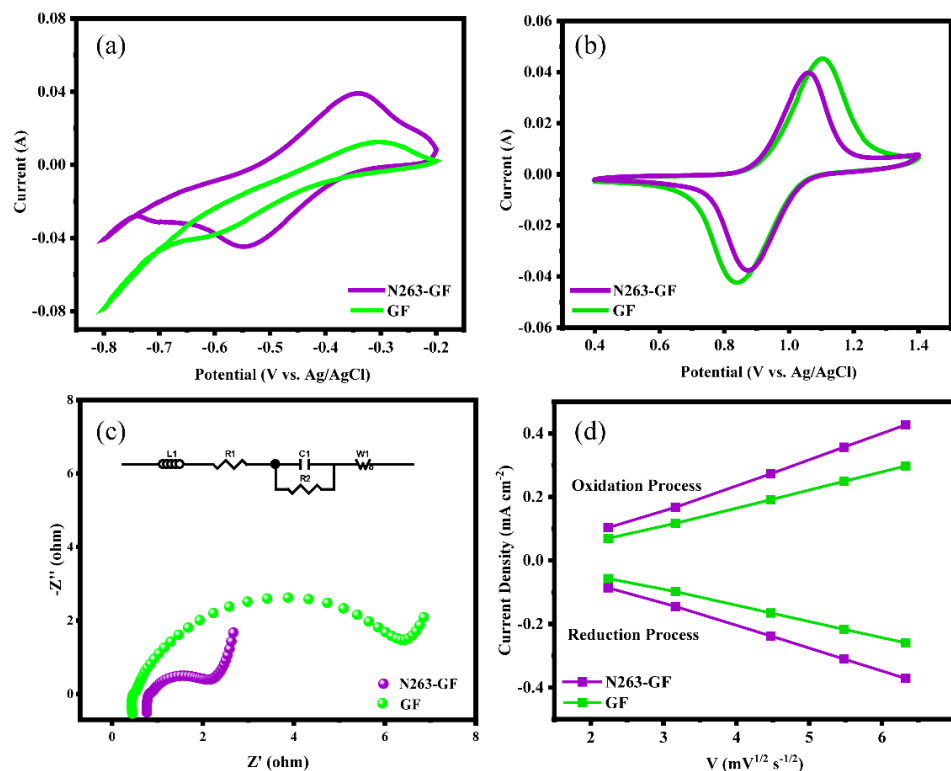


Figure 5. The negative electrode (a) and positive electrode (b) CV curves of the N263-GF, GF in $3 \text{ mol L}^{-1} \text{ H}_2\text{SO}_4$ solution containing $0.1 \text{ mol L}^{-1} \text{ VO}\text{SO}_4$ with scan rate of 10 mV/s , Equivalent circuit model, AC impedance spectrum (c) of N263-GF, GF, and positive electrode vanadium ion diffusion coefficient diagram (d) with scan rate of 5, 10, 20, 30, and 40 mV/s in $3 \text{ mol L}^{-1} \text{ H}_2\text{SO}_4$ solution containing $0.1 \text{ mol L}^{-1} \text{ VO}\text{SO}_4$.

Since i_p is proportional to $v^{1/2}$, the cyclic voltammetry test results, using different scan rates, yield the cyclic voltammetry peak currents and the square root of the scan rate for the GF and N263-GF positive electrodes, as can be seen in Figure 5d and Table S3, indicating that the N263-GF electrode with a larger slope is more favorable for ion transport. With an increasing scan rate, the ratio of the peak voltage difference to the peak current of the N263-GF electrode does not switch much; the apparent diffusion coefficient ($D_o = 8.8010 \cdot 10^{-12} \text{ cm}^2 \text{ s}^{-1}$, $D_r = 6.8110 \cdot 10^{-12} \text{ cm}^2 \text{ s}^{-1}$) derived from Equation (1) was larger than that of GF ($D_o = 4.3310 \cdot 10^{-12} \text{ cm}^2 \text{ s}^{-1}$, $D_r = 3.4510 \cdot 10^{-12} \text{ cm}^2 \text{ s}^{-1}$) which shows good stability and high reversible electrochemical performance.

Finally, we compared the VRFBs assembled with GF and N263-GF on the basis of charge and discharge tests under the same conditions, and it can be seen that the N263-GF (see Figure 6b) can operate stably at a current density of 300 mA cm^{-2} and still have high Coulomb efficiency (96.3%), energy efficiency (60.0%), and voltage efficiency (62.2%). In addition, from the energy efficiency in Figure 6c, it can be seen that the VRFBs assembled with N263-GF as the electrode exhibited a certain increase in energy efficiency compared to the vanadium redox battery assembled with GF, while the current density of the VRFBs assembled with GF was the limiting current density at 250 mA cm^{-2} , indicating that the polarization voltage increased at this time. As the battery side reactions intensify, the charging and discharging performance becomes unstable, and a short circuit can easily occur, resulting in battery damage. The capacity–voltage curve (Figure 6d) shows that the VRFBs assembled with N263-GF exhibited a relatively low charging plateau and

a relatively high discharging plateau at the current density of 200 mA cm^{-2} , and the overpotential of the battery assembled with N263-GF was reduced by 21% compared to GF. This result also demonstrates that the appropriate concentration of N263 doping can improve the electrochemical performance of the VRFBs, resulting in reduced polarization, an increased discharge capacity, and an increased charge transfer rate on the electrode surface. Moreover, the capacity efficiency of N263-GF VRFBs has a weakened decay of 0.2% after 1000 times constant current charge/discharge tests at the current density of 200 mA cm^{-2} (Figure 6e), which is 10.3% higher than the energy efficiency of the VRFBs assembled with GF electrodes. It is suggested that N263-GF has good long-cycle stability. In summary, the VRFBs assembled with N263-GF have an excellent charge and discharge performance, and it has more obvious advantages in reducing the concentration polarization and electrochemical polarization.

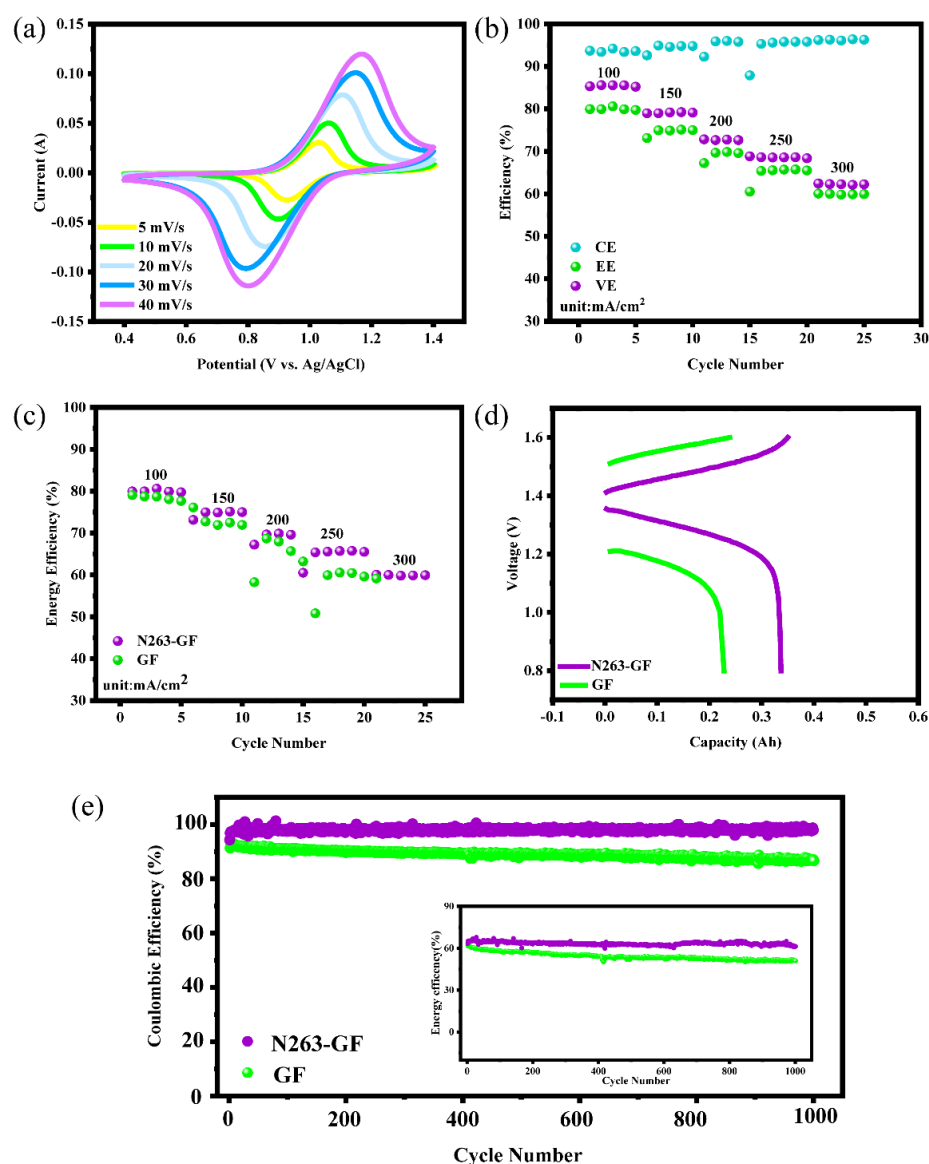


Figure 6. CV curves of N263-GF at different scan rates (a); charge/discharge multiplier test (b); energy efficiency comparison of N263-GF, GF in charge/discharge multiplier test (c); capacity voltage plots for current density of 200 mA cm^{-2} (d); long-cycle capacity efficiency and energy efficiency (e); and comparison of 200 mA cm^{-2} .

3. Materials and Methods

3.1. Materials

Electrolyte ($1.7 \text{ mol L}^{-1} \text{ V}^{3.5+}$, Yinfeng), deionized water, anhydrous ethanol (Maclean's, 99.7%), N263 (Maclean's, 97%), graphite mat (5.6 mm, $2 \text{ cm} \times 2 \text{ cm}$), and Nafion 115 proton exchange membrane (DuPont, $5 \text{ cm} \times 5 \text{ cm}$) were used.

3.2. Material Testing and Characterization

Field emission scanning electron microscopy (FEI Electron Optics B.V, Nova NanoSEM230) was used to examine the morphology of the N263-modified graphite felt electrode (N263-GF) and the blank control graphite felt (GF) electrode at a 15 kV voltage. By using XRD (Shimadzu, XRD-6000) at the 2θ range of $10\text{--}80^\circ$, 2° min^{-1} , the materials' crystalline structure and degree of graphitization were examined. A 532 nm laser was used to gather Raman (Horiba LabRAM HR Evolution) data to compare the level of flaws in the N263-GF electrode with the GF electrode. To investigate the BET (JW-BK100) properties and pore distribution of the materials, N_2 adsorption/desorption experiments were carried out at 77.35 K using a static volumetric method. An Al $K\alpha$ x-ray source of 1486.6 eV was used in XPS (Thermo Scientific K-Alpha) testing at a base pressure of 3×10^{-10} mbar to examine the elemental composition and distribution of the samples as well as the surface chemical functional groups. To examine the material's capabilities for immersion in solutions, a water contact angle meter (SDC 200S) was employed to record the contact angle established instantly by a drop of deionized water onto the sample surface.

A three-electrode system consisted of a platinum mesh as the auxiliary electrode, a $0.5 \text{ cm} \times 0.5 \text{ cm}$ graphite felt (GF) or modified graphite felt (N263-GF) as the working electrode, with Ag/AgCl as the reference electrode, and $0.1 \text{ mol L}^{-1} \text{ VOSO}_4$ prepared as the electrolyte using $3 \text{ mol L}^{-1} \text{ H}_2\text{SO}_4$ as the solvent. The CV curves were tested on CHI604E with a voltage range of 0.4–1.4 V and scan rates of 5, 10, 20, 30, and 40 mV/s. EIS tests were performed in a frequency range of 0.1–100 kHz with the open circuit voltage as the initial voltage and the amplitude as the amplitude of 5 mV. The AC impedance spectra were tested and fitted with Z-view software. A single VRFB was assembled with $2 \text{ cm} \times 2 \text{ cm}$ GF and N263-GF as the positive and negative electrodes, $1.7 \text{ mol L}^{-1} \text{ V}^{3.5+}$ 20 mL as the electrolyte, Nafion 115 as a proton exchange membrane at 25°C , a current density of 200 mA cm^{-2} , a charge/discharge voltage window of 0.8–1.6 V, and a Land charge/discharge tester (CT2001A). Long cycle life tests were performed, and constant current charge/discharge tests were performed at different current densities of $100\text{--}200 \text{ mA cm}^{-2}$, 0.95–1.55 V, $250\text{--}300 \text{ mA cm}^{-2}$, and 0.8–1.65 V.

3.3. Electrode Fabrication

To make the N263-GF electrode (Figure 7), N263 and anhydrous ethanol were first mixed together. Untreated graphite felt was then added to the mixture, and the mixture was then selected for 30 min. Then, it was allowed to dry for 12 h at 80°C . Secondly, argon-filled tube furnaces were used to heat the material to 600°C for 2 h, and it was maintained in muffle furnaces at 400°C for 5 h with an air atmosphere. The cooled graphite felt was then washed with deionized water, dried for 12 h at 80°C , and set aside.

For the preparation of the blank control graphite felt (GF) electrodes, untreated graphite felt was sonicated for 30 min while submerged in an anhydrous ethanol solution. The graphite felts were then dried for 12 h in an oven at 80°C . Second, argon-filled tube furnaces were used to heat the material to 600°C for 2 h, then muffle furnaces with an air atmosphere were used to maintain the material at 400°C for 5 h. Deionized water was used to clean the cooled graphite felt before it was dried and stored at 80°C for 12 h.

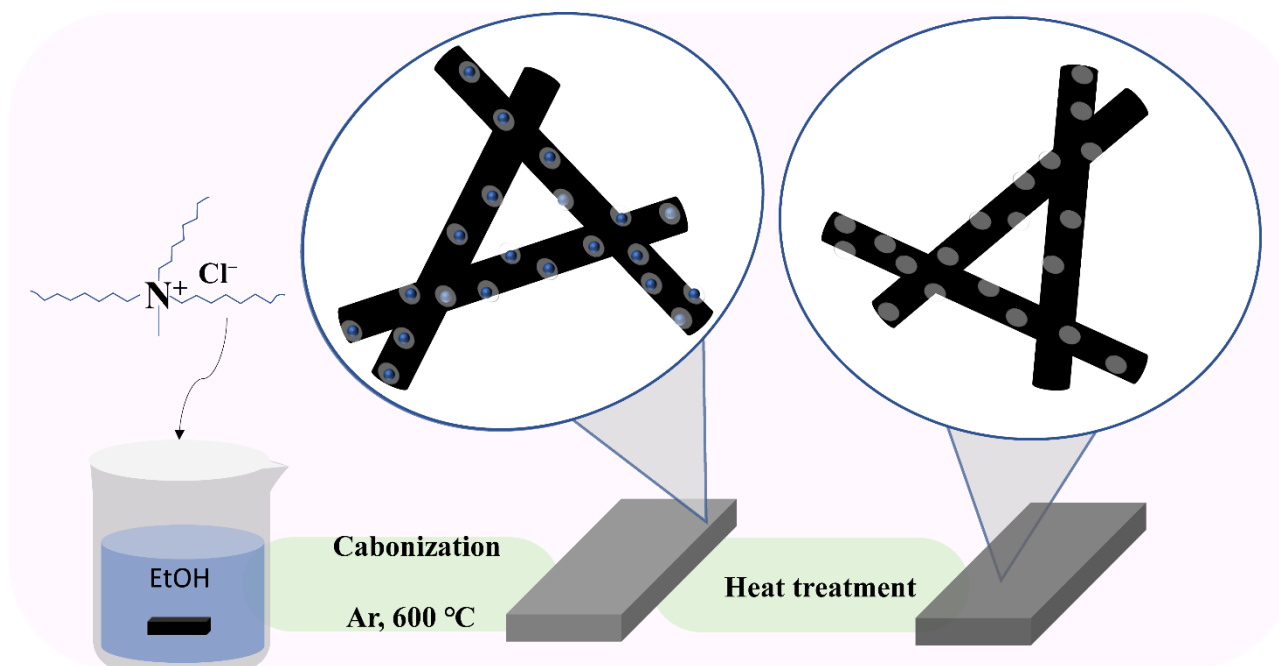


Figure 7. Schematic diagram of the preparation process for the N263-modified graphite felt (N263-GF) electrodes.

4. Conclusions

N263, as the nitrogen source, optimized the hydrophilic performance and electrocatalytic activity of the graphite felt electrode for VRFBs. The N doping was achieved under high-temperature conditions, and the elemental composition and functional group structure of the N263-GF surface were verified. Some nitrogen carbide particles were uniformly distributed on the surface of the nitrogen-doped graphite felt electrode materials, enhancing the electrochemical performance of the vanadium redox current battery to a certain extent. Notably, an excessive content may inhibit the charge transfer, so oxidation treatment is needed to solve these problems. After exploring these conditions, N and O on the surface of the electrode were found to act synergistically to catalyze the redox reaction of the vanadium ions while still ensuring good capacity retention and good stability during the 200 mA cm^{-2} charge/discharge process. This research provides a facile strategy to modify graphite felt electrodes for efficient VRFBs, which is of great significance for the development of grid-scale energy storage technology.

Supplementary Materials: The following supporting information can be downloaded at: <https://www.mdpi.com/article/10.3390/inorganics10110208/s1>, Figure S1: Results of multipoint BET specific surface area and mesoporous, microporous internal surface area tests on N263-GF, GF; Figure S2: Raman spectra of different regions of N263-GF (a, b, c) and GF (d, e, f); Table S1: Raman spectrometer test results in different regions of electrodes; Figure S3: Comparison of cyclic voltammetry tests at 10 mV/s for electrodes prepared under different conditions; Figure S4: AC impedance diagram of electrodes prepared under different conditions; Table S2: Values of the AC impedance equivalent circuit elements; Table S3: Positive electrode vanadium ion diffusion coefficient.

Author Contributions: X.L. and J.H. contributed equally to this work. X.W., X.L. and J.H. conceived the idea, designed the research plan, and wrote the paper. X.L. and H.L. carried out experiments and analyzed data. J.L. and S.F. contributed to discussion on the electrochemical performance. X.W., Y.W. and J.H. supervised the whole project. All authors have read and agreed to the published version of the manuscript.

Funding: This work was financially supported by the Hunan Provincial Science and Technology Innovation Major Project (Grant No. 2020GK1010-2020GK1014-4) and the Basic Science Center Project of the National Key R&D Program of China (Grant No. 2021YFB2400400).

Institutional Review Board Statement: The study did not require ethical approval.

Informed Consent Statement: Not applicable.

Conflicts of Interest: The authors declare no conflict of interest.

References

1. Lin, D.; Li, Y. Recent Advances of Aqueous Rechargeable Zinc-Iodine Batteries: Challenges, Solutions, and Prospects. *Adv. Mater.* **2022**, *34*, 2108856. [[CrossRef](#)] [[PubMed](#)]
2. He, Z.; Lv, Y.; Zhang, T.; Zhu, Y.; Dai, L.; Yao, S.; Zhu, W.; Wang, L. Electrode materials for vanadium redox flow batteries: Intrinsic treatment and introducing catalyst. *Chem. Eng. J.* **2022**, *427*, 131680. [[CrossRef](#)]
3. Vinco, J.H.; Domingos, A.E.E.d.C.; Espinosa, D.C.R.; Tenório, J.A.S.; Baltazar, M.d.P.G. Unfolding the Vanadium Redox Flow Batteries: An in-depth perspective on its components and current operation challenges. *J. Energy Storage* **2021**, *43*, 103180. [[CrossRef](#)]
4. Cheng, D.; Tian, M.; Wang, B.; Zhang, J.; Chen, J.; Feng, X.; He, Z.; Dai, L.; Wang, L. One-step activation of high-graphitization N-doped porous biomass carbon as advanced catalyst for vanadium redox flow battery. *J. Colloid Interface Sci.* **2020**, *572*, 216–226. [[CrossRef](#)] [[PubMed](#)]
5. Qiu, J.; Huang, B.; Liu, Y.; Chen, D.; Xie, Z. Glucose-derived hydrothermal carbons as energy storage booster for vanadium redox flow batteries. *J. Energy Chem.* **2020**, *45*, 31–39. [[CrossRef](#)]
6. Deng, Q.; Tian, Y.; Ding, P.; Yue, J.; Zeng, X.-X.; Yin, Y.-X.; Wu, X.-W.; Lu, X.-Y.; Guo, Y.-G. Porous lamellar carbon assembled from *Bacillus mycoides* as high-performance electrode materials for vanadium redox flow batteries. *J. Power Sources* **2020**, *450*, 227633. [[CrossRef](#)]
7. Hou, B.; Tang, R.; Zhang, Q.; Cui, X.; Chen, Y. Graphitization of carbon-based catalyst for improving the performance of negative electrode in vanadium redox flow battery. *Mater. Res. Express* **2021**, *8*, 045604. [[CrossRef](#)]
8. Busacca, C.; Blasi, O.D.; Giacompo, G.; Briguglio, N.; Antonucci, V.; Blasi, A.D. High performance electrospun nickel manganese on carbon nanofibers electrode for vanadium redox flow battery. *Electrochim. Acta* **2020**, *355*, 136755–136764. [[CrossRef](#)]
9. Sun, J.; Jiang, H.R.; Zhang, B.W.; Chao, C.Y.H.; Zhao, T.S. Towards uniform distributions of reactants via the aligned electrode design for vanadium redox flow batteries. *Appl. Energy* **2020**, *259*, 114198. [[CrossRef](#)]
10. He, Y.; Zhuang, X.; Lei, C.; Lei, L.; Hou, Y.; Mai, Y.; Feng, X. Porous carbon nanosheets: Synthetic strategies and electrochemical energy related applications. *Nano Today* **2019**, *24*, 103–119. [[CrossRef](#)]
11. Jiang, Y.; Cheng, G.; Li, Y.; He, Z.; Zhu, J.; Meng, W.; Zhou, H.; Dai, L.; Wang, L. Superior electrocatalytic performance of porous, graphitic, and oxygen-functionalized carbon nanofiber as bifunctional electrode for vanadium redox flow battery. *Appl. Surf. Sci.* **2020**, *525*, 146453. [[CrossRef](#)]
12. Daugherty, M.C.; Hsieh, C.-T.; Aaron, D.S.; Ashraf Gandomi, Y.; Li, J.; Zheng, Y.; Pflieger, W. Enabling high rate capability, low internal resistance, and excellent cyclability for vanadium redox flow batteries utilizing ultrafast laser-structured graphite felt. *Electrochim. Acta* **2020**, *344*, 136171. [[CrossRef](#)]
13. Sun, J.; Wu, M.C.; Fan, X.Z.; Wan, Y.H.; Chao, C.Y.H.; Zhao, T.S. Aligned microfibers interweaved with highly porous carbon nanofibers: A novel electrode for high-power vanadium redox flow batteries. *Energy Storage Mater.* **2021**, *43*, 30–41. [[CrossRef](#)]
14. Deng, Q.; HuangYang, X.Y.; Zhang, X.; Xiao, Z.H.; Zhou, W.B.; Wang, H.R.; Liu, H.Y.; Zhang, F.; Li, C.Z.; Wu, X.W.; et al. Edge-Rich Multidimensional Frame Carbon as High-Performance Electrode Material for Vanadium Redox Flow Batteries. *Adv. Energy Mater.* **2022**, *12*, 2103186. [[CrossRef](#)]
15. Wang, R.; Li, Y.; He, Y.-L. Achieving gradient-pore-oriented graphite felt for vanadium redox flow batteries: Meeting improved electrochemical activity and enhanced mass transport from nano- to micro-scale. *J. Mater. Chem. A* **2019**, *7*, 10962–10970. [[CrossRef](#)]
16. Kim, S.-C.; Lim, H.; Kim, H.; Yi, J.S.; Lee, D. Nitrogen and oxygen dual-doping on carbon electrodes by urea thermolysis and its electrocatalytic significance for vanadium redox flow battery. *Electrochim. Acta* **2020**, *348*, 136286–136299. [[CrossRef](#)]
17. He, Z.; Zhou, X.; Zhang, Y.; Jiang, F.; Yu, Q. Low-Temperature Nitrogen-Doping of Graphite Felt Electrode for Vanadium Redox Flow Batteries. *J. Electrochem. Soc.* **2019**, *166*, A2336–A2340. [[CrossRef](#)]
18. Jiang, Y.; Du, M.; Cheng, G.; Gao, P.; Dong, T.; Zhou, J.; Feng, X.; He, Z.; Li, Y.; Dai, L.; et al. Nanostructured N-doped carbon materials derived from expandable biomass with superior electrocatalytic performance towards V^{2+}/V^{3+} redox reaction for vanadium redox flow battery. *J. Energy Chem.* **2021**, *59*, 706–714. [[CrossRef](#)]
19. Chen, Z.; Gao, Y.; Zhang, C.; Zeng, X.; Wu, X. Surface-Wrinkle-Modified Graphite Felt with High Effectiveness for Vanadium Redox Flow Batteries. *Adv. Electron. Mater.* **2019**, *5*, 1900036–1900044. [[CrossRef](#)]
20. Radinger, H.; Ghamlouche, A.; Ehrenberg, H.; Scheiba, F. Origin of the catalytic activity at graphite electrodes in vanadium flow batteries. *J. Mater. Chem. A* **2021**, *9*, 18280–18293. [[CrossRef](#)]
21. Zhang, K.; Yan, C.; Tang, A. Oxygen-induced electrode activation and modulation essence towards enhanced anode redox chemistry for vanadium flow batteries. *Energy Storage Mater.* **2021**, *34*, 301–310. [[CrossRef](#)]

22. Gursu, H.; Gencten, M.; Sahin, Y. Synthesis of Phosphorus Doped Graphenes via the Yucel's Method as the Positive Electrode of a Vanadium Redox Flow Battery. *J. Electrochem. Soc.* **2021**, *168*, 060504. [[CrossRef](#)]
23. Wang, R.; Li, Y.; Wang, Y.; Fang, Z. Phosphorus-doped graphite felt allowing stabilized electrochemical interface and hierarchical pore structure for redox flow battery. *Appl. Energy* **2020**, *261*, 114369. [[CrossRef](#)]
24. Park, S.E.; Yang, S.Y.; Kim, K.J. Boron-functionalized carbon felt electrode for enhancing the electrochemical performance of vanadium redox flow batteries. *Appl. Surf. Sci.* **2021**, *546*, 148941. [[CrossRef](#)]
25. Dresselhaus, M.S.; Jorio, A.; Hofmann, M.; Dresselhaus, G.; Saito, R. Perspectives on carbon nanotubes and graphene Raman spectroscopy. *Nano Lett.* **2010**, *10*, 751–758. [[CrossRef](#)]
26. Jorio, A.; Saito, R. Raman spectroscopy for carbon nanotube applications. *J. Appl. Phys.* **2021**, *129*, 021102. [[CrossRef](#)]
27. Zheng, Y.; Deng, T.; Yue, N.; Zhang, W.; Zhu, X.; Yang, H.; Chu, X.; Zheng, W. Raman spectroscopy and correlative-Raman technology excel as an optimal stage for carbon-based electrode materials in electrochemical energy storage. *J. Raman Spectrosc.* **2021**, *52*, 2119–2130. [[CrossRef](#)]
28. Xu, Y.; Zhang, C.; Zhou, M.; Fu, Q.; Zhao, C.; Wu, M.; Lei, Y. Highly nitrogen doped carbon nanofibers with superior rate capability and cyclability for potassium ion batteries. *Nat. Commun.* **2018**, *9*, 1720. [[CrossRef](#)]
29. Ling, W.; Deng, Q.; Ma, Q.; Wang, H.R.; Zhou, C.J.; Xu, J.K.; Yin, Y.X.; Wu, X.W.; Zeng, X.X.; Guo, Y.G. Hierarchical Carbon Micro/Nanonetwork with Superior Electrocatalysis for High-Rate and Endurable Vanadium Redox Flow Batteries. *Adv. Sci.* **2018**, *5*, 1801281. [[CrossRef](#)]
30. Liu, S.; Tian, J.; Wang, L.; Zhang, Y.; Qin, X.; Luo, Y.; Asiri, A.M.; Al-Youbi, A.O.; Sun, X. Hydrothermal treatment of grass: A low-cost, green route to nitrogen-doped, carbon-rich, photoluminescent polymer nanodots as an effective fluorescent sensing platform for label-free detection of Cu(II) ions. *Adv. Mater.* **2012**, *24*, 2037–2041. [[CrossRef](#)]
31. Park, M.; Ryu, J.; Kim, Y.; Cho, J. Corn protein-derived nitrogen-doped carbon materials with oxygen-rich functional groups: A highly efficient electrocatalyst for all-vanadium redox flow batteries. *Energy Environ. Sci.* **2014**, *7*, 3727–3735. [[CrossRef](#)]
32. Alazmi, A.; Wan, C.T.-C.; Costa, P.M.F.J.; Brushett, F.R. Exploration of reduced graphene oxide microparticles as electrocatalytic materials in vanadium redox flow batteries. *J. Energy Storage* **2022**, *50*, 104192. [[CrossRef](#)]
33. An, H.; Noh, C.; Jeon, S.; Shin, M.; Kwon, Y.; Chung, Y. The effect of low-defected carboxylic acid functional group-rich carbon nanotube-doped electrode on the performance of aqueous vanadium redox flow battery. *Int. J. Energy Res.* **2022**, *46*, 11802–11817. [[CrossRef](#)]
34. Yoon, S.J.; Kim, S.; Kim, D.K.; Yu, D.M.; Hempelmann, R.; Hong, Y.T.; So, S. Nitrogen-Doping Through Two-Step Pyrolysis of Polyacrylonitrile on Graphite Felts for Vanadium Redox Flow Batteries. *Energy Fuels* **2020**, *34*, 5052–5059. [[CrossRef](#)]
35. Vujković, M.; Gavrilov, N.; Pašti, I.; Krstić, J.; Travas-Sejdic, J.; Ćirić-Marjanović, G.; Mentus, S. Superior capacitive and electrocatalytic properties of carbonized nanostructured polyaniline upon a low-temperature hydrothermal treatment. *Carbon* **2013**, *64*, 472–486. [[CrossRef](#)]
36. Li, O.L.; Chiba, S.; Wada, Y.; Panomsuwan, G.; Ishizaki, T. Synthesis of graphitic-N and amino-N in nitrogen-doped carbon via a solution plasma process and exploration of their synergic effect for advanced oxygen reduction reaction. *J. Mater. Chem. A* **2017**, *5*, 2073–2082. [[CrossRef](#)]
37. Dang, H.X.; Barz, D.P.J. Graphene electrode functionalization for high performance hybrid energy storage with vanadyl sulfate redox electrolytes. *J. Power Sources* **2022**, *517*, 230712. [[CrossRef](#)]
38. Ersozoglul, M.G.; Gursu, H.; Gencten, M.; Sarac, A.S.; Sahin, Y. A new approach to prepare N-/S-doped free-standing graphene oxides for vanadium redox flow battery. *Int. J. Energy Res.* **2022**, *46*, 19992–20003. [[CrossRef](#)]
39. Faggiano, L.; Lacarbonara, G.; Badenhorst, W.D.; Murtomäki, L.; Sanz, L.; Arbizzani, C. Short thermal treatment of carbon felts for copper-based redox flow batteries. *J. Power Sources* **2022**, *520*, 230846. [[CrossRef](#)]
40. Wang, F.; Zhang, P.; Wang, G.; Nia, A.S.; Yu, M.; Feng, X. Functional Electrolytes: Game Changers for Smart Electrochemical Energy Storage Devices. *Small Sci.* **2021**, *2*, 2100080. [[CrossRef](#)]
41. Liu, X.; Cheng, Q.; Zhong, W.; Deng, Q.; Yang, C.; Liu, Y.; Hu, J.; Yang, C. Construction of defective $\text{Mo}_x\text{W}_{1-x}\text{S}_2/\text{Cu}_7.2\text{S}_4$ polyhedral heterostructures for fast sodium storage. *Chem. Eng. J.* **2023**, *451*, 138645. [[CrossRef](#)]
42. Xu, W.; Long, J.; Liu, J.; Luo, H.; Duan, H.; Zhang, Y.; Li, J.; Qi, X.; Chu, L. A novel porous polyimide membrane with ultrahigh chemical stability for application in vanadium redox flow battery. *Chem. Eng. J.* **2022**, *428*, 131203. [[CrossRef](#)]
43. Shi, Y.; Wei, Z.; Liu, H.; Zhao, J. Dynamic modeling of long-term operations of vanadium/air redox flow battery with different membranes. *J. Energy Storage* **2022**, *50*, 104171. [[CrossRef](#)]
44. Ko, Y.; Park, H.; Lee, B.; Bae, Y.; Park, S.K.; Kang, K. A comparative kinetic study of redox mediators for high-power lithium-oxygen batteries. *J. Mater. Chem. A* **2019**, *7*, 6491–6498. [[CrossRef](#)]